High Energy Density Nanocomposites Based on Surface-Modified $BaTiO_3$ and a Ferroelectric Polymer

Philseok Kim,[†] Natalie M. Doss,[†] John P. Tillotson,[†] Peter J. Hotchkiss,[†] Ming-Jen Pan,[§] Seth R. Marder,[†] Jiangyu Li,[‡] Jeffery P. Calame,[§] and Joseph W. Perry[†,*]

[†]School of Chemistry and Biochemistry and Center for Organic Photonics and Electronics, Georgia Institute of Technology, 901 Atlantic Drive, Atlanta, Georgia 30332, [‡]Department of Mechanical Engineering, University of Washington, Stevens Way, Box 352600, Seattle, Washington 98195, and [§]Naval Research Laboratory, 4555 Overlook Avenue, Washington, D.C. 20375

ABSTRACT The dielectric permittivity and electric breakdown strength of nanocomposites comprising poly(vinylidene fluoride-*co*-hexafluoro propylene) and phosphonic acid surface-modified $BaTiO_3$ nanoparticles have been investigated as a function of the volume fraction of nanoparticles. The mode of binding of pentafluorobenzylphosphonic acid on the $BaTiO_3$ particles was investigated using infrared and ^{31}P solid-state nuclear magnetic resonance spectroscopy, and the phosphonic acid was found to form well ordered, tightly bound monolayers. The effective permittivity of nanocomposites with low volume fractions (<50%) was in good agreement with standard theoretical models, with a maximum relative permittivity of 35. However, for nanoparticle volume fractions of greater than 50%, the effective permittivity was observed to decrease with increasing nanoparticle volume fraction, and this was correlated with an increase in porosity of the spin-coated nanocomposite films. The dielectric breakdown strength was also found to decrease with increasing volume fraction of the $BaTiO_3$ nanoparticles, with an abrupt decrease observed around 10% and a gradual decrease for volume fractions of 20—50%. Comparison of these results with model calculations, using statistical particle packing simulations and effective medium theory for the permittivity and breakdown strength, indicates the important roles of nanoparticle percolation and porosity of the nanocomposites on the dielectric properties. The measured energy density at a field strength of 164 V/μm, well below the breakdown strength, increased to a value of 3.2 J/cm^3 as the nanoparticle volume fraction is increased to 50%, roughly in line with the trend of the permittivity. The calculated maximum energy densities indicate maximal extractable energy (7—8 J/cm^3 at 1 kHz) for two different particle volume fractions, as a result of the interplay of the dependencies of permittivity and breakdown strength on volume fraction.

KEYWORDS: dielectric nanocomposite · barium titanate · surface modification · permittivity · dielectric breakdown · energy storage

Polymer—metal oxide nanocomposites are currently of considerable interest as solution processable high-permittivity materials for electronic applications such as embedded capacitors, multilayer capacitors, high-energy-density capacitors, and gate insulators in organic field effect transistors.[1−5] These nanocomposites can have both high permittivity and high dielectric strength and can be solution processed on large and flexible substrates at low temperatures and ambient pressures. However, the high surface energy of dielectric nanoparticles usually leads to agglomeration and phase separation from the polymer host matrix, resulting in poor processability of the films and a high defect density.

Recently, we have shown that surface modification of $BaTiO_3$ and other perovskite nanoparticles with functional phosphonic acids can allow the formation of high quality nanocomposite films that exhibit good solution processability, low leakage current, high permittivity, and high dielectric strength.[1,5] Previous studies suggest that the volume fraction of the high permittivity component (nanoparticle filler) has to be increased above a certain threshold (usually 30%) to increase the effective permittivity of the nanocomposite.[2,6,7] However, increasing the volume fraction of nanoparticles typically decreases the apparent dielectric strength of the nanocomposite owing to the enhancement of the local electric field in the host material.[8,9] Therefore, the filler volume fraction of a nanocomposite should be rationally optimized in order to maximize the stored energy density.

Ferroelectric polymers based on poly(vinylidene fluoride) and its copolymers are considered to be useful materials for energy storage because of their large permittivities and dielectric strengths.[10−15] However, their large dielectric loss (~10%) limits their use in applications that require fast charge/discharge cycles in the 100 kHz−1 MHz frequency range. Therefore, the combination of high permittivity nanoparticles with low loss and a ferroelectric polymer host can potentially provide high permittivity, high dielectric strength, and low loss nanocomposite materials that retain

See the accompanying Perspective by Ducharme on p 2447.

*Address correspondence to joe.perry@gatech.edu.

Received for review June 17, 2009 and accepted July 28, 2009.

Published online August 5, 2009. 10.1021/nn9006412 CCC: $40.75

comparable processability to polymeric materials. However, nanocomposites with a large volume fraction of nanoparticles can exhibit porosity[16] that is detrimental to their dielectric performance.[7] This raises the question of what is the optimum volume fraction of a nanocomposite that gives the maximum extractable energy at a certain frequency. In this regard, we investigated the role of the volume fraction of high permittivity nanoparticles on the dielectric properties (permittivity, dielectric loss, and breakdown strength) of nanocomposites in order to determine the optimum volume fraction(s).

Herein we report a systematic study of the effect of nanoparticle volume fractions on the dielectric properties of nanocomposites based on phosphonic acid-modified $BaTiO_3$ (BT) and poly(vinylidene fluoride-*co*-hexafluoropropylene) (P(VDF-HFP)). The surface modification of BT with a fluorinated phosphonic acid has been investigated using FT-IR, thermogravimetric analysis, and solid-state NMR spectroscopy to determine the coverage and the nature of the binding of the phosphonic acid ligand. The morphology of the BT/P(VDF-HFP) nanocomposites was investigated using scanning electron microscopy to probe for the presence of air voids in high volume fraction composites. The frequency dependent dielectric permittivities and loss, and the DC-breakdown strength of the nanocomposites as a function of nanoparticle volume fraction are reported. We have employed self-consistent effective medium theory (SC-EMT) and statistical particle packing simulations with finite difference calculations to model the dielectric properties of nanocomposites with a wide range of nanoparticle volume fractions, including possible air voids, the results of which showed good agreement with the experimental data. On the basis of these studies, guidelines for the optimization of dielectric nanocomposites for energy storage applications are presented.

CALCULATION OF EFFECTIVE PERMITTIVITY AND BREAKDOWN STRENGTH OF NANOCOMPOSITES

The nanocomposites studied herein can be considered as a 0−3-type composite of high permittivity nanoparticle fillers discretely distributed in a continuous dielectric polymer matrix. Simple composite medium theories, such as the Kerner model, treat the dielectric filler particles as polarizable spheres, in which dipoles are induced under an applied electric field. The reduction in electric field within the high permittivity filler particles is considered, but the effect of the particles on the field in the host medium is neglected. The effective permittivity, ε_{eff}, is calculated using an average of the host and the filler particle permittivities, wherein the contributions are weighted by the volume fraction and the field in each component, as given below:

$$\varepsilon_{eff} = \frac{\varepsilon_h f_h + \varepsilon_f f_f (E_{fz}/E_{hz})}{f_h + f_f (E_{fz}/E_{hz})} \quad (1)$$

where ε_h, f_h, and ε_f, f_f are the permittivities and the volume fractions of the host and filler, respectively, and E_f and E_h are the fields in the respective components.[17] Other commonly used composite models include the Clausius−Mossotti and Maxwell Garnet treatments, and the Lichtenecker logarithmic law of mixing,[18−20] all of which have been shown to reasonably predict the dielectric properties of composites at relatively low volume fraction, ≤20%.[21] These simple models do not take into account the influence of the particle−particle dipolar interactions or their effect on the surrounding medium, which become important at higher volume fractions.

To better model the effective permittivity of a composite system at high filler volume fractions, Jayasundere and Smith (JS) developed a modified Kerner model that accounts for dipolar interactions between pairs of neighboring spherical filler particles, which leads to a modified local field in the medium[6] and results in the following expression for the effective permittivity:

$$\varepsilon_{eff} = \frac{\varepsilon_h f_h + \varepsilon_f f_f (A)(B)}{f_h + f_f (A)(B)} \quad (2)$$

where

$$A = \frac{3\varepsilon_h}{\varepsilon_f + 2\varepsilon_h}$$

and

$$B = 1 + \frac{3 f_f (\varepsilon_f - \varepsilon_h)}{\varepsilon_f + 2\varepsilon_h}$$

An alternative approach to the calculation of the effective permittivity and the breakdown strength of a nanocomposite over a wide range of volume fractions is the use of self-consistent effective medium theory (SC-EMT). With SC-EMT, the effects of interactions between neighboring particles and the inclusion of possible air voids in the composite can be readily modeled as a three component (host, particles, and air voids) system.[22] This model incorporates the effects of introducing high dielectric constant fillers into a lower dielectric matrix, which can produce localized hot spots of increased electric field concentration in the host. The effective permittivity (ε_{eff}) is expressed as

$$\varepsilon_{eff} = \varepsilon_1 + f_2(\varepsilon_2 - \varepsilon_1)a_2 + f_3(\varepsilon_3 - \varepsilon_1)a_3 \quad (3)$$

where the host matrix, filler, and possible voids represent phases 1, 2, and 3, respectively, and a_r denotes the electric-field concentration factor in each phase, r. The electric field concentration factor relates the average electric field in phase r to an applied electric field E_0 as $\langle E_r \rangle = a_r E_0$. The effective medium approximation provides a reasonable estimate of a_r which is expressed as[22]

$$a_r = 1 - s[(\varepsilon_r - \varepsilon_{eff})^{-1}\varepsilon_{eff} + s]^{-1}, \quad r = 2,3 \qquad (4)$$

where s is the depolarization factor and is $^1/_3$ for spherical particles. The field concentration factor for the host matrix can be determined from the normalization condition:

$$\sum_{r=1}^{3} f_r a_r = 1 \qquad (5)$$

Using eqs 4 and 5, eq 3 is solved self-consistently for ε_{eff}.

The inclusion and interaction of high permittivity filler particles in a host matrix induces an enhancement of the average field in polymer host, $\langle E_1 \rangle$, which in turn reduces the apparent dielectric breakdown strength. One criterion for the apparent breakdown strength is based on the average field in the host polymer

$$\langle E_1 \rangle = a_1 E_0 \geq E_b \qquad (6)$$

where E_b is the breakdown field of the pure host polymer. Because dielectric breakdown is a statistical process that is subject to spatial fluctuations in the local field, the above criterion that simply uses an average field overestimates the breakdown strength and thus is not sufficiently accurate to reasonably predict breakdown fields. Therefore, the statistical fluctuation of the average field has been taken into account for more accurate breakdown field predictions.[23]

$$\langle E_1 \rangle + \sqrt{\langle E_1^2 \rangle - \langle E_1 \rangle^2} \geq E_b \qquad (7)$$

where

$$\langle E_1^2 \rangle = \frac{1}{f_1}\frac{\partial \varepsilon_{eff}}{\partial \varepsilon_1} E_0^2$$

With this approach, the apparent breakdown criterion becomes

$$E_0\left(a_1 + \sqrt{\frac{1}{f_1}\frac{\partial \varepsilon_{eff}}{\partial \varepsilon_1} - a_1^2}\right) \geq E_b \qquad (8)$$

RESULTS AND DISCUSSION

Surface Modification of BT for Incorporation in Fluoropolymer Host. $BaTiO_3$ (BT) nanoparticles tend to form large aggregates because of their high surface energy and large surface area, which can lead to a highly inhomogeneous film when simply blended in a polymer matrix. To mitigate this problem for incorporation of BT into a fluoropolymer matrix, poly(vinylidene fluoride-*co*-hexafluoropropylene) (P(VDF-HFP)), BT nanoparticles (30−50 nm, Aldrich) were surface modified using a fluorinated organophosphonic acid ligand, pentafluorobenzyl phosphonic acid (PFBPA), in an ethanol/water mixture (Figure 1). The surface-modified BT nanoparticles (PFBPA−BT) were washed thoroughly to remove

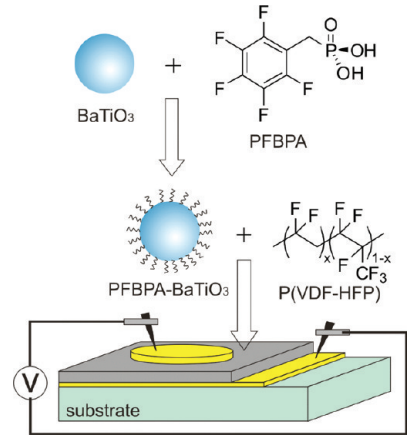

Figure 1. Schematic illustration of surface modification of BT, nanocomposite formation, and the geometry of fabricated nanocomposite thin film capacitors.

excess ligand, then mixed with P(VDF-HFP) in *N,N*-dimethylformamide (DMF) at a known volume ratio.

To characterize the surface modification of the BT nanoparticle surface with the PFBPA ligand, FT-IR and ^{31}P solid-state NMR (SS-NMR) spectra were recorded. The binding of phosphonic acids to the BT surface is reflected in the changes in the FT-IR spectra before and after the surface modification (Figure 2). The aromatic skeletal vibration modes at 1502 and 1528 cm^{-1} and the C−F stretching mode at 1126 cm^{-1} of PFBPA were detected in PFBPA-modified BT nanoparticles. There was a significant reduction in the intensity of surface hydroxyl stretching (3400−3500 cm^{-1}) of the BT nanoparticles and the broad free-hydrogen-bonded (P)O−H stretching mode (2240−2380 cm^{-1}) implying the condensation of surface hydroxyl groups of BT and the hydroxyl groups of PFBPA in the surface modification reaction. In the fingerprint region, the initially complex pattern of P═O (1200 cm^{-1}) and P−O (1090−990 cm^{-1}) stretching modes collapses to two major peaks at 1095 and 1045 cm^{-1} that are assigned as the asymmetric and symmetric P−O−M (M = surface metal) stretching modes.[5,24]

^{31}P solid-state NMR (SS-NMR) revealed further details of the binding modes of PFBPA on the BT surface (Figure 3). Large chemical shifts were observed between unbound PFBPA (δ = 27.9 ppm) and bound PFBPA (δ = 20.8 and 14.5 ppm) on BT. The majority of bound PFBPA was associated with peaks centered at δ = 14.5, δ = 17.0, and δ = 20.6 ppm. The largest change in chemical shift from free PFBPA to bound PFBPA on the BT nanoparticle surface was 13.4 ppm. This change is close to the value for octylphosphonic acid binding to BT surface ($\Delta\delta$ = 14.3 ppm), which has been assigned as a combination of tridentate and bidentate configurations.[5] The other peak is interpreted as the less associated monodentate configuration. There was no evidence of phosphonate gel that might have been formed by a self-condensation reaction, which would be expected to appear as a sharp peak around −4.0 to

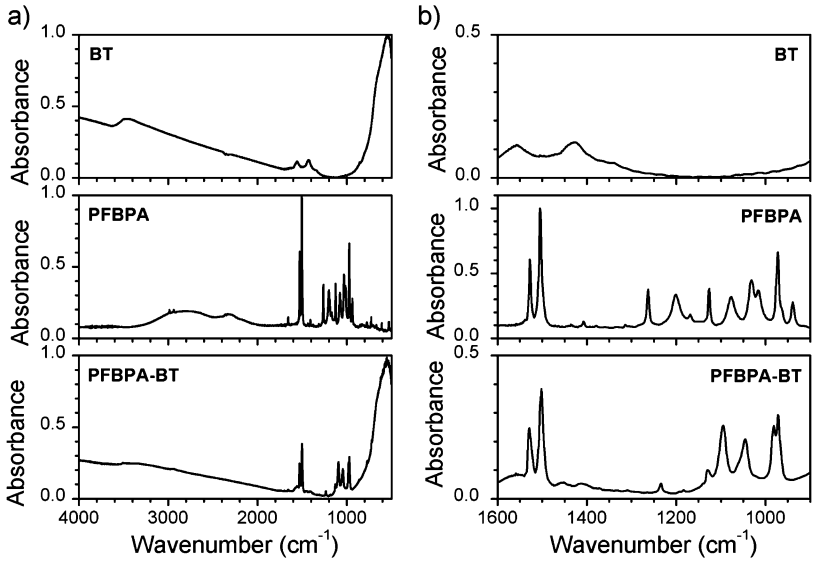

Figure 2. FT-IR absorption spectra of unmodified BT, PFBPA, and PFBPA-BT. (a) Wide range spectra and (b) expanded view of P−O stretching region. The spectra for BT and PFBPA−BT were normalized using the lattice Ti−O absorption peak centered at ~540 cm^{-1}. The spectrum of PFBPA was normalized using the maximum absorption peak.

−7.0 ppm.[25] Long-chain alkyl phosphonic acids binding to the BT nanoparticle surface are known to form densely packed crystalline-like layers, upon which the C−H stretching peaks shift to smaller wavenumbers in FT-IR spectrum. The alkyl phosphonic acids loosely bound to the BT nanoparticle surface do not seem to form crystalline-like layers, since they are detected only in the direct-polarization ^{31}P SS-NMR, and are not enhanced in the cross-polarization method. In contrast, PFBPAs binding to the BT nanoparticle surface appear to form crystalline-like layers, irrespective of the binding mode, as all of the ^{31}P peaks are detected in the cross-polarization experiment. This is attributed to the strong π−π interaction between adjacent PFBPA molecules.

To determine the surface coverage of PFBPA on BT nanoparticles, measurements of the BET specific surface area of dried and unmodified BT nanoparticles (25.8 m^2/g) and thermogravimetric analysis of both BT and PFBPA-BT nanoparticles were performed. The net weight loss from the surface bound PFBPA was found to be 3.49%, which corresponds to 76% of a theoretical monolayer, assuming that the footprint of each phosphonic acid is 24 Å^2 (Figure 4).[26]

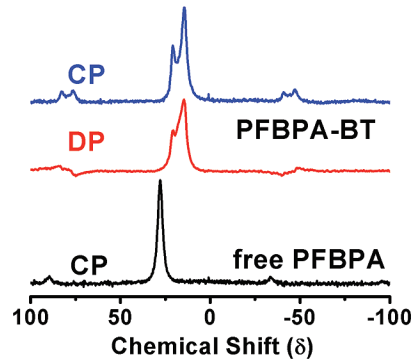

Figure 3. ^{31}P MAS SS-NMR spectra of free PFBPA (black, cross-polarization) and PFBPA-BT (blue, cross-polarization and red, direct polarization).

The surface-modified BT particles formed a homogeneous dispersion in P(VDF-HFP)/DMF solution after ball-milling the mixture. In this study, no additional dispersant was used in the processing of the nanocomposites of surface-modified BT nanoparticles. Surface modification had a dramatic effect on the stability of the nanocomposite dispersions and improved the quality of nanocomposite films produced by spin coating.

The microscopic homogeneity of the nanocomposite films was investigated by imaging the top surface and the freeze-fractured cross sections of nanocomposite films using a scanning electron microscope (SEM). Figure 5 shows the SEM images of the top surfaces and the freeze-fractured cross sections of PFBPA-BT:P(VDF-HFP) nanocomposite films. The surface-modified BT nanoparticles with PFBPA formed uniform and high quality nanocomposite thin films in the P(VDF-HFP) host.

Dielectric Characterization of PFBPA−BT:P(VDF-HFP) Nanocomposites. The effective permittivities of the PFBPA−BT:P(VDF-HFP) nanocomposites were determined using dielectric spectroscopy for films with varying volume fractions of nanoparticles. The results are compared with the values obtained from several models in Figure 6. The experimental permittivity values gradually increased with increasing nanoparticle volume fraction followed by a maximum in the permittivity at around 50−60%, after which the permittivity decreased rapidly with further increase of the nanoparticle volume fraction. A large discrepancy between observed and calculated permittivities was observed at

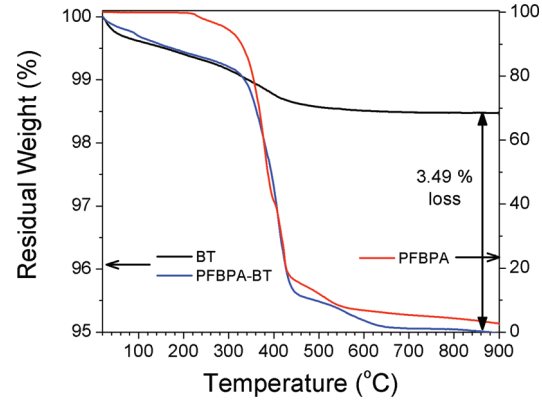

Figure 4. Thermogravimetric analysis of dried and unmodified BT (black), PFBPA-BT (blue), and PFBPA (red). Note that the scale of weight loss for BT and PFBPA-BT is the left *Y*-axis and the scale of weight loss for PFBPA is the right *Y*-axis.

volume fractions above 60%, as associated with the decrease in the experimentally observed permittivities.

Figure 7 shows the results of dielectric spectroscopy measurements on the nanocomposites with varying volume fractions of BT over the frequency range of 20 Hz to 1 MHz. The dielectric loss is expressed as the loss tangent (tan δ), also known as the dissipation factor, which is defined as the ratio of the imaginary part to the real part of the permittivity ($\varepsilon''/\varepsilon'$). The dielectric spectroscopy for the PFBPA−BT:P(VDF-HFP) films for each nanoparticle volume fraction revealed that the dielectric loss is mainly due to a resonance of the host material,[28,29] as evidenced by the strong reduction in loss as a function of BT particle volume fraction. The BT nanoparticles used in this study have an average diameter of 30−50 nm and their crystalline phase was identified as cubic phase (paraelectric) by powder X-ray diffraction (see Supporting Information). It is generally accepted that the Curie temperature of BT at this size is slightly above room temperature with very small dielectric anomaly.[30,31] The dispersion of the loss becomes very small as the BT volume fraction approaches 80% and, concomitantly, the frequency dependence of the dielectric constant becomes quite flat. At a BT volume fraction of 80% the loss at 1 kHz is ~0.01 and at 1 MHz is about 0.02, showing that the loss associated with the phosphonic acid-coated BT nanoparticles is very low. The P(VDF-HFP) host polymer contains less than 15% HFP, according to the manufacturer specification, and the films of it exhibited relaxor ferroelectric behavior in the temperature range 40−70 °C that matches well with a previously published result with 14% HFP.[29] However, this behavior was almost unnoticeable with the addition of 50% vol. of PFBPA−BT (see Supporting Information). This is attributed to the interactions of the nanoparticles with the polymer matrix that interferes the segmental motion or alters the semicrystalline structure of the ferroelectric polymer host, which would otherwise contribute to the relaxor ferroelectric behavior in the same temperature range.

The dielectric breakdown strength was also measured for the nanocomposites with BT volume fractions from 0 to 50% and analyzed using Weibull statistics.[32,33] The Weibull analysis is based on an empirical failure probability distribution that is typically described using three parameters:

$$P_F(E) = 1 - \exp[-\{(E-\gamma)/\alpha\}^{\beta}] \quad (9)$$

where α is a scale parameter, β is a shape parameter that shows dispersion of E, and γ is a threshold parameter below which value of E no failure occurs. For the analysis of breakdown results of nanocomposites in this study, γ was set to zero. The failure probability can then be expressed as

$$\log[-\ln\{1 - P_F(E)\}] = \beta \log E - \beta \log \alpha \quad (10)$$

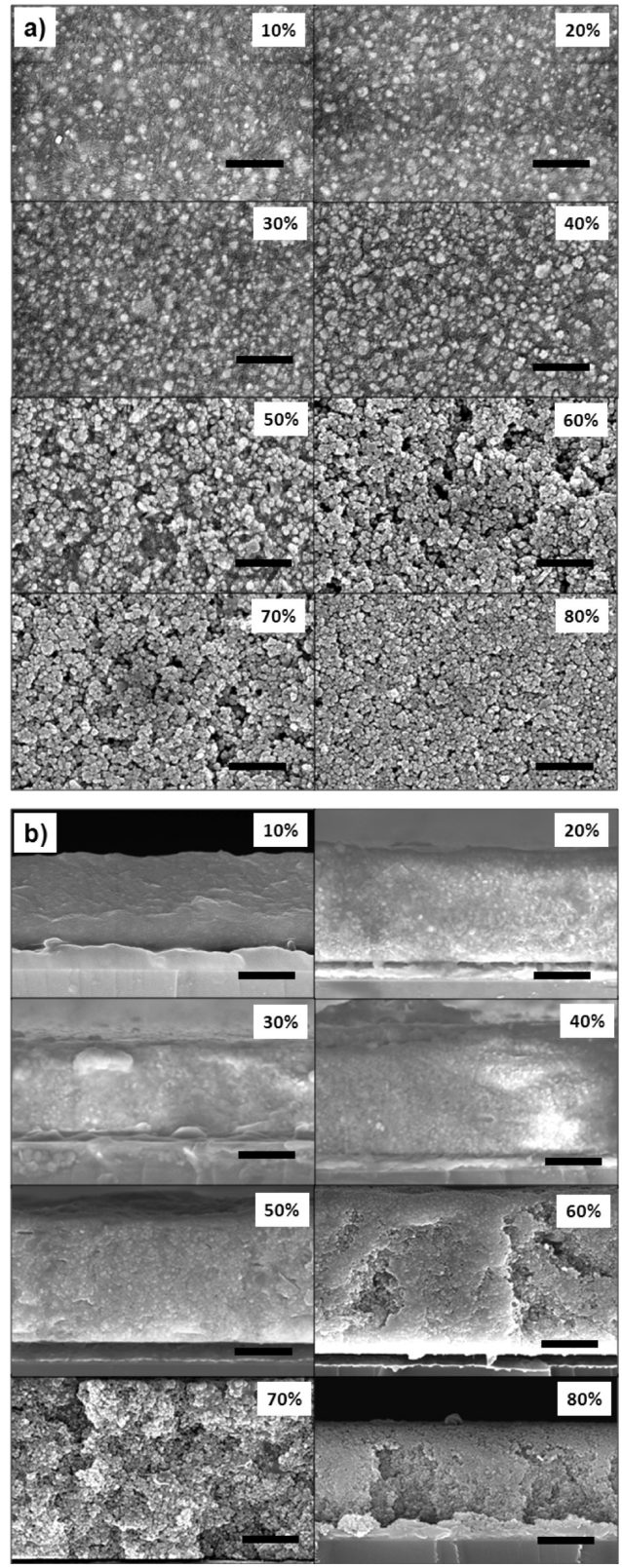

Figure 5. (a) SEM images of top surfaces of PFBPA-BT:P(VDF-HFP) nanocomposite films with different nanoparticle volume fractions. Scale bars are 300 nm. (b) SEM images of the freeze-fractured cross sections of PFBPA−BT:P(VDF−HFP) nanocomposite films with different nanoparticle volume fractions. Scale bars are 1 μm.

This probability is equated with a median ranked positioning which is expressed as[34]

$$P_F(i,n) = [(i - 0.3)/(n + 0.4)] \times 100 \qquad (11)$$

where i is the index (1, 2, 3,..., n) and n is the sample size. The measured n (typically $n > 20$ in this study) breakdown field values (E) are reordered in ascending order and then the failure probability, P_F(E), for each E is given from the positioning equation. A linear fitting of $\log\{-\ln(1 - P)\}$ *vs* log E gives the parameters α and β. The breakdown field for the data set is found to be $E_B = \alpha$ when the failure probability is 63.2% (*i.e.*, $1 - 1/e$). These parameters can be inserted into eq 9 to find the cumulative distribution function (CDF) which represents the probability of failure as a function of applied field (Figure 8). Samples with volume fractions of 5% and 15% were also prepared and measured to better resolve the dielectric behavior of the nanocomposite around 10% volume fraction. These results were reproduced within the error range from a few separate batches of samples.

The breakdown behavior of high volume fraction (>50%) nanocomposites is thought to be closely related to the increase in the volume fraction of air voids, which will significantly lower the breakdown strength of the nanocomposites due to the low breakdown strength of air (~3 V/μm).[35] The breakdown strengths for the nanocomposites above 50% volume fraction varied strongly from sample to sample, likely due to the significant and randomly distributed porosity in the nanocomposites, and thus consistent values were not obtained from the analysis. The effect of porosity on the dielectric properties of the nanocomposites will be discussed below.

The results in Figure 8b clearly show that the breakdown strength (at a failure probability of 63.2%) decreases upon addition of BT nanoparticles to the host material as expected. It should be noted that there is a

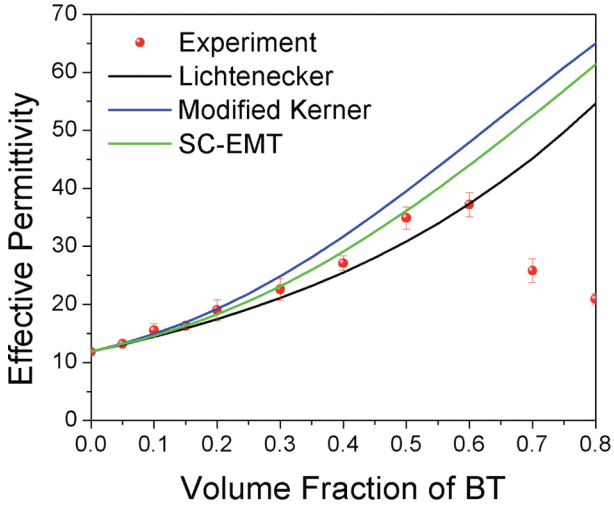

Figure 6. Comparison of measured effective relative permittivity (at 1 kHz) of nanocomposites as a function of PFBPA−BT nanoparticle volume fraction with predicted values from different theoretical models. Permittivity values used were 80 for PFBPA−BT nanoparticles and 11.9 for the polymer host.[27]

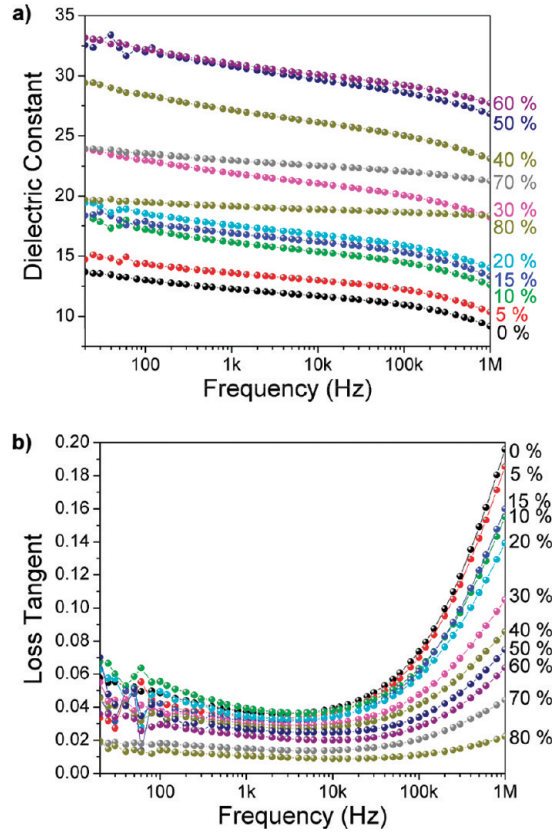

Figure 7. Dielectric spectroscopy of each PFBPA−BT:P(VDF-HFP) nanocomposite from 20 Hz to 1 MHz: dielectric constant (a) and the loss tangent (b). The dielectric loss gradually increases with increasing frequency and it is mainly due to a resonance of the polymer host.

sudden decrease in the dielectric strength when the volume fraction changes from 10 to ~20%. Similar trends have been observed in previous work, although an explanation of the behavior was not provided.[8,9] Our interpretation of this behavior is based on percolation of the BT nanoparticles in the composite. As previously described by Calame,[7] the percolation of particles in a composite can be viewed as occurring in two different regimes: the "soft" percolation and the "hard" percolation regimes. In the soft percolation regime, where extended networks of connected particles begin to form, a percolative pathway consisting of contacted particles that span across the nanocomposite thin film can be formed. When this soft percolation occurs, then the breakdown strength will be abruptly reduced, as the charge conduction along the percolative pathways can occur, facilitating breakdown. This effect appears to be effectively suppressed with the use of surface-modified nanoparticles, owing in part to the passivation and reduction in the number of ionizable surface sites by the phosphonate layer. As a result, the magnitude of the drop in the breakdown strength in this regime can be mitigated as compared to the nanocomposites with unmodified nanoparticles. In our study, the onset of such a percolation pathway appears to occur between the volume fractions of BT of 10 and 20%. With a further in-

crease of the nanoparticle volume fraction, "hard" percolation can take place, in which the local packing density of the particles reaches a maximum. At this point, most of the particles are in contact with neighboring particles and the further addition of particles does not increase the particle density. The composites may undergo a relaxation process to find a denser packing configuration to reduce the local concentration of air voids, but this process is typically kinetically controlled, as in the spin-coating film fabrication process. Increasing the particle/polymer ratio in an effort to increase the volume fraction of the particles results only in the creation of localized air voids in the composite, owing to an insufficient amount of polymer to fill the interstitial free volume generated by the random packing of the particles. Therefore, the dielectric breakdown strength decreases and is strongly dependent on the local distribution of the air voids. Since the particles are typically randomly packed, the air void distribution is also random and thus the breakdown behavior shows a large statistical variation.

Another interesting observation is that the failure probability of a pure P(VDF-HFP) film at moderate fields is higher than those of nanocomposites with 5% and 10% PFBPA−BT (Figure 8a). This implies that doping of the polymer host with high permittivity filler under the "soft" percolation threshold can reduce the failure probability under moderate fields at which the capacitors may be operated. Even under a relatively low applied electric field, there is a finite probability for carrier generation inside the nanocomposite film that may lead to breakdown. The high permittivity nanoparticles can act as traps for these charges and also effectively scatter charges in the nanocomposite film, that results in the reduction of the failure probability. This result is somewhat similar to a previous observation by Tuncer et al., who reported that doping poly(vinyl alcohol) with 10−30 wt % TiO_2 nanoparticles makes the dielectric breakdown behavior more reproducible and improves the breakdown characteristics.[36]

The Effect of Porosity. The discrepancy between the experimental and model calculation results for the effective relative permittivities at high volume fractions shown in Figure 6 is attributed mainly to the porosity in the nanocomposite film. When this occurs, the nanocomposite is no longer a 0−3 composite since the polymer phase is no longer a continuous phase in all three directions. Consequently, the porosity effect at high filling ratios should be taken into account in the treatment of the effective permittivity.

The volume fraction of air voids as a function of the intended nanoparticle volume fraction has been computed previously using a statistical cellular packing model along with finite difference calculations.[7] We have used such simulations in this study in order to calculate the maximum volume fraction of nanoparticles that is achievable without creating air voids and the

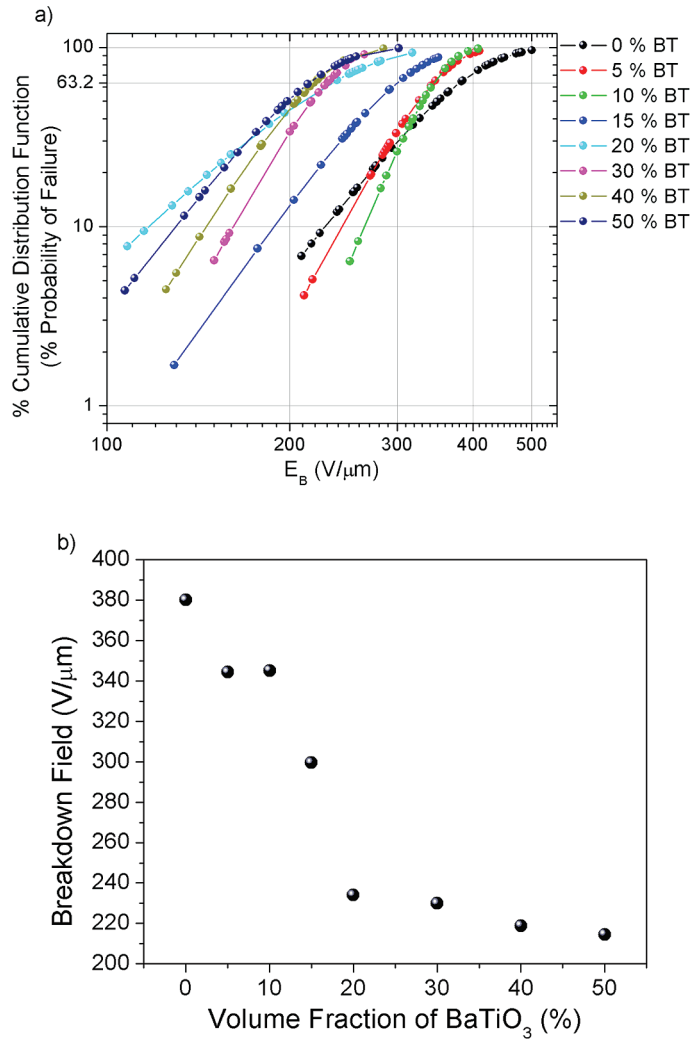

Figure 8. (a) Percent cumulative distribution function (% probability of device failure) of each nanocomposite as a function of applied electric field and (b) the breakdown strengths (failure probabilities: 63.2%) at each volume fraction as determined from the Weibull analysis.

void volume dependence on intended particle volume fraction. The simulation used a model space with 200 cubical cells per each *x*, *y*, and *z* axis. These cells were filled with dielectric spheres that have a radius of 15 cells. When filling the space with spheres, partial spheres were also allowed near the edges, as long as the center of the sphere was located within the model space. Once a particle was placed, the center position was not allowed to move (*i.e.*, the particle was "frozen" and no relaxation processes were allowed). Therefore, the models do not represent a maximally dense composite. In this particular simulation, the maximally filled model space contained 283 particles including partial particles, corresponding to a particle volume fraction of 0.397. This threshold corresponds to the maximum particle volume fraction, for which there are no air voids inside the composite. Any further addition of particles would be accompanied by the creation of voids, as the particles are not allowed to undergo relaxation to form a denser composite. Representative packings of par-

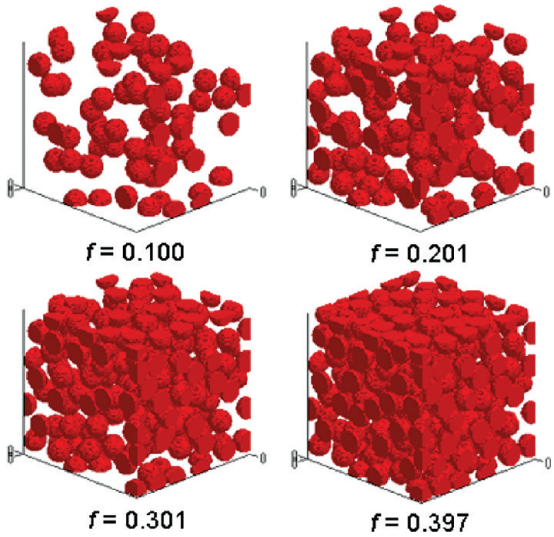

Figure 9. Examples of particle packing in finite difference simulations at different volume fractions. Note that at $f = 0.397$, a maximal number of spherical particles has been placed in a given model space and no additional particle can be added to this model space. The intended increase of particle volume fraction over $f = 0.397$ can only be made by decreasing the volume of host polymer, which inevitably creates air voids.

ticles in a model space at selected volume fractions are shown in Figure 9.

The total volume fraction of air voids for a given particle volume fraction was obtained by fitting the air void volume simulation result to a polynomial function with a threshold volume fraction (f_T) for the onset of the air void formation given below:

$$V(F) = a(f - f_T)^p \qquad (12)$$

where f is the volume fraction, f_T is the threshold volume fraction below which no void is formed ($f_T = 0.397$ from finite difference simulation), and a and p are fitting parameters. Using this void volume function, the actual volume fractions of each constituent (nanoparticle, host, and air void) as a function of intended nanoparticle volume fraction were calculated, and these values were used in the SC-EMT calculation to obtain the dielectric properties shown in Figure 10.

The void volume fraction function based on the finite difference simulation overestimated the amount of air voids as indicated by the premature and rapid decrease of the effective permittivity. This is due to differences in particle density between the fabricated films and the statistical packing simulation. The films were fabricated by spin coating, which is a kinetically controlled process. However, the films were also thermally treated to allow the relaxation of nanoparticles to reduce porosity and improve the quality of the films. This can effectively shift the threshold volume fraction for the appearance of air voids to a higher volume fraction than that obtained from the simulation. The SEM images in Figure 5 show that the porosity is not significant up to 50% nanoparticle volume fraction and the

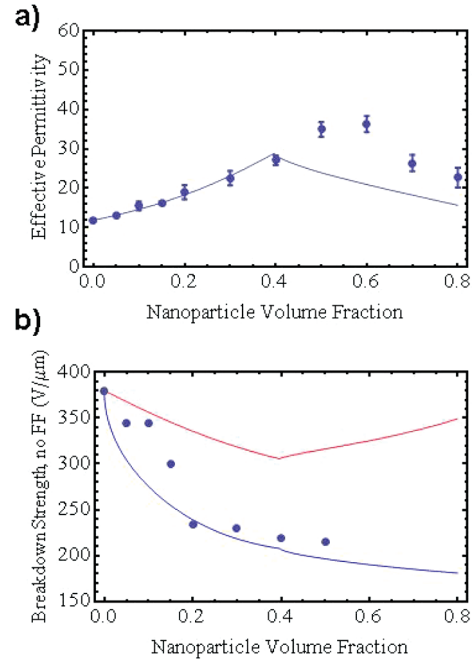

Figure 10. Comparison of (a) permittivities at 1 kHz and (b) breakdown strengths predicted by combined self-consistent effective medium approximation and finite difference simulation (lines) with experimental values (dots). The breakdown calculation results without field fluctuation and with field fluctuation are shown in red and blue, respectively.

porosity is obvious above 60% of nanoparticles. On the basis of this observation, the threshold volume fraction (f_T) in eq 12 was adjusted to a more realistic value of 0.55.

Breakdown strengths predicted without considering the field fluctuations in the medium are overestimated in comparison to the experimental results. When the field fluctuations were taken into account, the calculated results were reasonably close to the experimental values but still did not show the sudden decrease at around 10% nanoparticle volume fraction.

Figure 11 shows the calculated volume fractions of each constituent with an adjusted threshold volume fraction ($f_T = 0.55$). Using the adjusted porosity threshold volume fraction, the SC-EMT calculation resulted in

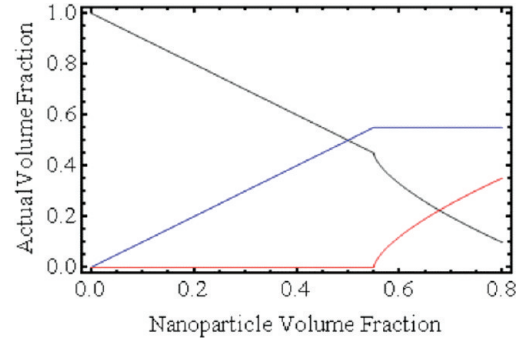

Figure 11. The calculated volume fractions of nanoparticle (blue), polymer (black), and the air voids (red) as functions of intended nanoparticle volume fraction with adjusted threshold volume fraction of nanoparticles (0.55) for air void creation.

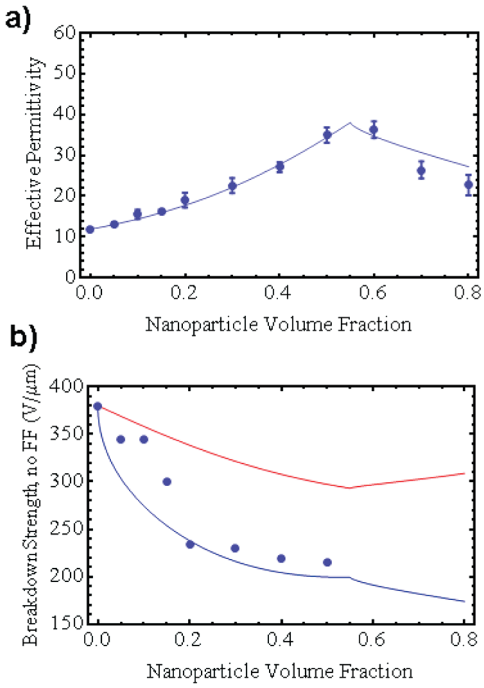

Figure 12. Comparison of relative permittivities at 1 kHz (a) and breakdown strengths (b) predicted by combined self-consistent effective medium approximation and finite difference simulation (lines) with experimental values (dots) after adjusting the onset volume fraction based on SEM observation. The breakdown calculation results without field fluctuation and with field fluctuation are shown in red and blue, respectively.

a better agreement with the experimental values as shown in Figure 12.

It should also be noted that the size of the crystalline domains of the P(VDF-HFP) host were observed to decrease with increasing nanoparticle volume fraction, as evidenced by the SEM images (Figure 5a) and decreased peak intensities associated with the ordered microstructures of P(VDF-HFP) in X-ray diffractograms of the nanocomposites (see Supporting Information), and as might be expected given the effect smaller interparticle distances would have on the formation of the crystalline domains during processsing. This observation has implications for particle volume fraction dependence of both the permittivity and the energy density of the nanocomposite. We have not accounted for this effect in the modeling of the nanocomposite permittivity but we expect that it would lead to a reduction in the apparent host permittivity as the nanoparticle volume fraction is increased. This is consistent with the experimental permittivity values of the nanocomposites at very high particle volume fraction being somewhat lower than what is predicted by the SC-EMT calculations that do not account for any change in the host polymer permittivity.

Therefore, the combined self-consistent effective medium theory and the finite difference simulation of the particle packing provide a reasonably good approach to model the dielectric properties of nanocomposites, especially those with high nanoparticle volume fractions where air voids have a significant role. However, it should be noted that the sudden drop of the breakdown strength at ~10% volume fraction of nanoparticles was not very well predicted by this model. For particle volume fractions of 5−15%, the model predicts a drop in breakdown strength that is more rapid than the experimental data. This may be the result of charge trapping or scattering that impedes breakdown as discussed above in regard to the breakdown probability at lower voltages for neat P(VDF-HFP) compared to low volume fraction nanocomposites. Such effects could lead to a higher breakdown strength than predicted for the composites in the 5−15% volume fraction range. The experimental breakdown strengths do show a significant drop with increasing volume fraction between 10 and 20% which we believe is related to the onset of soft percolation. Breakdown requires a continuous percolative pathway between the local breakdown sites through the film.[37] In a randomly packed nanocomposite, the average number of neighboring nanoparticles can be assumed to be approximately 10.[38] Therefore, if there is at least 1 breakdown occurring out of 10 neighboring sites, then avalanche breakdown can readily take place. This can be modeled by using the finite difference simulation, through which the probability of the electric field enhancement relative to the applied electric field can be calculated. If we define the breakdown criteria as the local field exceeding the breakdown strength of pure host material, then the breakdown strength of the nanocomposites can be approximately calculated when the applied field induces about 10% probability of the local field exceeding the breakdown strength of the host material.

Optimization of Volume Fraction for Maximum Energy Density. The expression for the maximum energy storage density of a capacitor is given by

$$U_{max} = \frac{1}{2}\varepsilon_0\varepsilon_{eff}E_B^2 \qquad (13)$$

where ε_{eff} is the effective permittivity of the composite and E_B is the breakdown field strength. To have a maximum energy density, the nanoparticle volume fraction in a nanocomposite should be rationally chosen in such a way that the combination of the effective permittivity and the breakdown strength gives the maximum value of energy density. The maximum energy storage densities of the nanocomposite capacitors at each volume fraction of PFBPA−BT were calculated using eq 13. Actual energy densities were also measured using a charge−discharge circuit under a fixed moderate field well below the breakdown field strength. These energy density values are compared in Figure 13.

The calculations indicate that a large maximum energy storage density, ≥5.4 J/cm^3 at 1 MHz, may possibly be obtained with PFBPA−BT:P(VDF-HFP) nanocomposites for nanoparticle volume fractions of 10% and

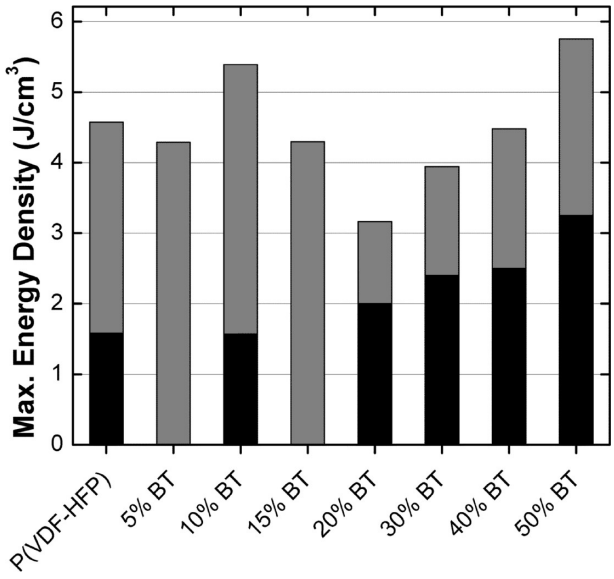

Figure 13. Calculated maximum energy storage density (gray) and measured energy density (black) of PFBPA−BT:P(VDF-HFP) nanocomposites with different nanoparticle volume fractions. The permittivity values measured at 1 MHz and the DC breakdown strength were used for calculated energy density. Energy densities were measured under a fixed applied field of 164 V/μm.

50%. At a frequency of 1 kHz, the calculated maximum energy density is 8 and 7 J/cm^3, at 10% and 50% respectively. This energy density is in the range of the value (6.9 J/cm^3) recently reported by Li *et. al* for 10% volume fraction of 30−50 nm TiO_2 nanorods dispersed in a ferroelectric vinylidene fluoride-based terpolymer, for which the relative permittivity is ~45.[15] The measured energy density values showed a similar trend as the calculated values but were somewhat lower than the calculated values. This is because the energy density measurements are limited by the breakdown and once samples break down, energy densities at higher fields cannot be measured. This limits the allowable breakdown probability to more like 10−20%. Accordingly, the measured energy density is considerably lower than what is calculated based on the probability of breakdown chosen in the statistics. Energy densities measured at the same applied field (164 V/μm) showed a general trend of increase in energy density up to 50% followed by a decreasing trend due to the presence of air voids discussed earlier (data not shown). It should be noted that all the nanocomposites showed a quadratic increase of energy density with increasing electric field, indicating that the permittivity of all nanocomposites remained constant up to the point of breakdown without dielectric saturation (see Supporting Information). In contrast, the onset of dielectric saturation is clear for pure P(VDF-HFP) at fields of 350−400 V/μm or higher. Therefore, the dielectric saturation of the barium titanate nanoparticles is not a limiting factor for the measured energy densities of nanocomposites (see Supporting Information).

Another important factor to consider in these types of nanocomposite is the dielectric loss. Typically, high-energy-density capacitors are used in pulsed power applications requiring high frequency operation conditions. Dielectric materials with a large dielectric loss tend to dissipate a fraction of their stored energy in the form of heat, which can be detrimental to the device performance as thermally facilitated breakdown can occur. Therefore, the 50% PFBPA−BT:P(VDF-HFP) nanocomposite may be desirable for applications that require low loss characteristics. However, considering the energy storage per weight and the mechanical properties of the nanocomposite films, a relatively low volume fraction could be desirable. In this case, the 10% nanoparticle volume fraction seems to be the optimum volume fraction for PFBPA−BT:P(VDF-HFP) nanocomposites. The study of the effect of the nanoparticle volume fraction thus provides a guideline to find an optimum nanoparticle volume fraction depending on the specific application.

CONCLUSIONS AND OUTLOOK

The volume fraction of nanoparticles has a significant effect on both the effective permittivity and the dielectric breakdown strength of PFBPA−BT:P(VDF-HFP) nanocomposites. Calculations based on various models for the permittivity of composite materials agreed reasonably well with the experimental findings when no significant porosity was present in the nanocomposites (particle volume fractions up to 50%). At high nanoparticle volume fractions (>50%), for which there were significant volume fractions of air void, there was a decrease of the effective permittivity. The breakdown strength showed a significant decrease for particle volume fractions between 10 and 20%. The trends for the permittivity and breakdown strength over the range of volume fractions studied were reasonably well described by accounting for air voids *via* a statistical packing model and using a self-consistent effective medium to calculate the properties of the resulting three phase (polymer, particles, and air voids) system. Calculations gave distinct values of the volume fraction (10% and 50%) of BT nanoparticles in PFBPA−BT:P(VDF-HFP) nanocomposites with maximal extractable energy densities, with values as high as 7−8 J/cm^3 at 1 kHz, as a result of the different trends for the permittivity and breakdown strength. On the other hand, the measured energy densities at a fixed field strength, well below breakdown, were found to show a monotonic increase with a maximum energy density of ~3.2 J/cm^3 for the composite with a 50% BT nanoparticle volume fraction. Efforts are underway to fabricate large area capacitor devices based on the developed nanocomposites, making use of processing methods that can reduce porosity, and to investigate nanocomposite compositions based on higher permittivity nanoparticles and polymer hosts as a path to higher energy densities. The suc-

cess of such efforts, as well as development of approaches to mitigate dielectric breakdown in nanocomposite materials, could pave the way to wide ranging applications that take advantage of the energy storage potential and processability of metal oxide−polymer nanocomposites.

METHODS

Surface Modification and Characterization. Chemicals were obtained from the following commercial sources and used without further purification: $BaTiO_3$ (BT, 30−50 nm: "nanosize-powder", Aldrich), poly(vinylidene fluoride-*co*-hexafluoropropylene) (P(VDF-HFP), cat. no. 427187, pellets with less than 15% of HFP, Aldrich). All other solvents were reagent grade and used without further purification.

Pentafluorobenzyl phosphonic acid (PFBPA) was synthesized by the Arbuzov reaction of pentafluorobenzyl bromide followed by hydrolysis with bromotrimethylsilane. PFBPA modified BT (PFBPA-BT) was prepared using a method reported previously.[5] In a typical reaction, 10 g of BT nanoparticles was dispersed in 250 mL mixture of 95:5 (v/v) ethanol/H_2O by an ultrasonic processor. A 3.28 g (12.5 mmol) portion of PFBPA dissolved in 10 mL of solvent was added to the BT dispersion. The mixture was ultrasonicated for 10 min and stirred at 80 °C for 1 h. The nanoparticles were separated by centrifugation and rinsed repeatedly with excess ethanol using ultrasonication at 30−40 °C for 30 min followed by centrifugation. After washing, the nanoparticles were dried overnight under vacuum at 80 °C.

Fourier transform infrared (FT-IR, Perkin-Elmer Spectrum 1000) spectra were obtained by using the KBr pellet method with 2 cm^{-1} resolution. BET gas adsorption/desorption analysis of unmodified BT and thermogravimetric analysis (TGA, TA Instruments, model TA 2950) of PFBPA-BT were used to calculate the surface coverage. The ^{31}P magic angle spinning (MAS) solid state NMR (SS-NMR) spectra were recorded on a Bruker DSX 400 (161.98 kHz ^{31}P frequency, 10 kHz MAS frequency, 256 scans, 10 s delay time) for both direct polarization (DP, 5 μs 90° pulse length, high power ^1H decoupling) and cross-polarization (CP, 1 ms contact time) experiments. The chemical shift was referenced using ammonium dihydrogen phosphate (ADP) which was set to $\delta = 1$ ppm.

Processing and Characterization of Nanocomposite Thin Films. Nanocomposites were prepared by ball-milling PFBPA−BT in *N*,*N*-dimethylformamide for 2 days, then P(VDF-HFP) was added and the mixture was further ball-milled for 12 days. Thin films of the nanocomposite were fabricated by spin-coating the dispersions on an aluminum-coated glass substrate as the base electrode. The aluminum surface was pretreated by using a cold plasma treatment with 3 SCFH (standard cubic feet per hour; 1 cubic foot ≈ 28.3 L) air at 750 W for 10 min. The films were soft baked on a hot plate (70−80 °C) for a few minutes then slowly cooled to room temperature. The films were subsequently dried *in vacuo* at 120 °C for an overnight period then slowly cooled to room temperature. The thickness of the films after drying was measured by using a contact profilometer (Dektac 6M, Veeco). The film morphology was imaged by using a field-emission scanning electron microscope (Zeiss Ultra60, WD = 4 mm, 5 kV) after gold sputter-coating. The cross-sectional images of the films were prepared by fracturing liquid-nitrogen cooled films.

Device Fabrication and Characterization. Parallel-plate capacitors were fabricated by depositing an array of circular (0.25 and 1.0 mm^2) top Al electrodes (500 nm thick) on the dielectric nanocomposite thin films through a shadow mask by using a thermal evaporator (model PVD75, Kurt J. Lesker) at 3 Å/s deposition rate. Frequency-dependent capacitance and loss tangent (dissipation factor) were measured by using an Agilent 4284A LCR meter from 20 Hz to 1 MHz at 1 V_{rms} with a parallel equivalent circuit. Dielectric breakdown strength was measured using a Keithley 248 high-voltage supply by sweeping the applied voltage from 50 V_{DC} at approximately 10 V/sec until the point of catastrophic device failure, as evidenced by spurious current changes and pitting of the top electrode.

Energy Density Measurement by Charge−Discharge. A charge−discharge circuit was used to measure the energy storage in dielectric samples. A schematic of the measurement setup is provided in Supporting Information. The sample (DUT) was first charged to the desired voltage using a high voltage power supply (Trek model 610D) through a high voltage relay (Kilovac KC-16). Immediately after charging, the relay was switched to connect the sample to a pair of current-monitoring resistors ($R1 \gg R2$). The voltage drop $V(t)$ across $R2$ was measured on an oscilloscope. An operational amplifier circuit (unity gain) with >1 $T\Omega$ input impedance was used to prevent current leakage through oscilloscope terminals. The total discharged energy was calculated using the following equation: Energy $= (R1 + R2)/(R2^2) \int_0^t V^2(t)\, dt$. The discharge time was typically on the order of milliseconds to tens of milliseconds, depending on the sample characteristics (permittivity, thickness, etc.).

Acknowledgment. This material is based upon work supported in part by the Office of Naval Research (N00014-05-1-0760) and by the STC Program of the National Science Foundation under Agreement No. DMR-0120967. This work was performed in part at the Microelectronics Research Center at the Georgia Institute of Technology, a member of the National Nanotechnology Infrastructure Network, which is supported by NSF (Grant No. ECS-03-35765). P.K. is grateful to LG Chem for financial support. We thank Profs. Bernard Kippelen and Angus Wilkinson for use of equipment in their laboratories.

Supporting Information Available: Supplementary figures and data. This material is available free of charge *via* the Internet at http://pubs.acs.org.

REFERENCES AND NOTES

1. Kim, P.; Zhang, X.-H.; Domercq, B.; Jones, S. C.; Hotchkiss, P. J.; Marder, S. R.; Kippelen, B.; Perry, J. W. Solution-Processible High-Permittivity Nanocomposite Gate Insulators for Organic Field-Effect Transistors. *Appl. Phys. Lett.* **2008**, *93*, 013302.
2. Rao, Y.; Qu, J.; Marinis, T.; Wong, C. P. A Precise Numerical Prediction of Effective Dielectric Constant for Polymer-Ceramic Composite Based on Effective-Medium Theory. *IEEE Trans. Adv. Packag. Technol.* **2000**, *23*, 680–683.
3. Ramesh, S.; Shutzberg, B. A.; Huang, C.; Gao, J.; Giannelis, E. P. Dielectric Nanocomposites for Integral Thin Film Capacitors: Materials Design, Fabrication and Integration Issues. *IEEE Trans. Adv. Packag.* **2003**, *26*, 17–24.
4. Schroeder, R.; Majewski, L. A.; Grell, M. High-Performance Organic Transistors using Solution-Processed Nanoparticle-Filled High-K Polymer Gate Insulators. *Adv. Mater.* **2005**, *17*, 1535–1539.
5. Kim, P.; Jones, S. C.; Hotchkiss, P. J.; Haddock, J. N.; Kippelen, B.; Marder, S. R.; Perry, J. W. Phosphonic Acid-Modified Barium Titanate Polymer Nanocomposites with High Permittivity and Dielectric Strength. *Adv. Mater.* **2007**, *19*, 1001–1005.
6. Jayasundere, N.; Smith, B. V. Dielectric Constant for Binary Piezoelectric 0−3 Composites. *J. Appl. Phys.* **1993**, *73*, 2462–2466.
7. Calame, J. P. Finite Difference Simulations of Permittivity and Electric Field Statistics in Ceramic-Polymer Composites For Capacitor Applications. *J. Appl. Phys.* **2006**, *99*, 084101.
8. Huang, C.; Zhang, Q. Enhanced Dielectric and Electromechanical Responses in High Dielectric Constant All-Polymer Percolative Composites. *Adv. Funct. Mater.* **2004**, *14*, 501–506.

9. Gilbert, L. J.; Schuman, T. P.; Dogan, F. In Dielectric Powder/Polymer Composites for High Energy Density Capacitors. *Advances in Electronic and Electrochemical Ceramics*; Proceedings of the 107th Annual Meeting of The American Ceramic Society, Baltimore, MD; Dogan, F., Kumta, P. N., Eds.; Wiley: Baltimore, MD, 2005.
10. Zhang, Q. M.; Bharti, V.; Zhao, X. Giant Electrostriction and Relaxor Ferroelectric Behavior in Electron-Irradiated Poly(vinylidene fluoride-trifluoroethylene) Copolymer. *Science* **1998**, *280*, 2101–2104.
11. Bai, Y.; Cheng, Z.-Y.; Bharti, V.; Xu, H. S.; Zhang, Q. M. High-Dielectric-Constant Ceramic-Powder Polymer Composites. *Appl. Phys. Lett.* **2000**, *76*, 3804–3806.
12. Chu, B.; Zhou, X.; Ren, K.; Neese, B.; Lin, M.; Wang, Q.; Bauer, F.; Zhang, Q. M. A Dielectric Polymer with High Electric Energy Density and Fast Discharge Speed. *Science* **2006**, *313*, 334–336.
13. Faria, L. O.; Welter, C.; Moreira, R. L. Relaxor Ferroelectric Behavior of Poly(Vinylidene Fluoride-Trifluoroethylene) Copolymer Modified by Low Energy Irradiation. *Appl. Phys. Lett.* **2006**, *88*, 192903.
14. Ranjan, V.; Yu, L.; Nardelli, M. B.; Bernholc, J. Phase Equilibria in High Energy Density PVDF-Based Polymers. *Phys. Rev. Lett.* **2007**, *99*, 047801.
15. Li, J.; Seok, S. I.; Chu, B.; Dogan, F.; Zhang, Q.; Wang, Q. Nanocomposites of Ferroelectric Polymers with TiO_2 Nanoparticles Exhibiting Significantly Enhanced Electrical Energy Density. *Adv. Mater.* **2009**, *21*, 217–221.
16. Schulze, K. A.; Zaman, A. A.; Soderholm, K.-J. M. Effect of Filler Fraction on Strength, Viscosity and Porosity of Experimental Compomer Materials. *J. Dent.* **2003**, *31*, 373–382.
17. Kerner, E. H. The Electrical Conductivity of Composite Media. *Proc. Phys. Soc. London, Sec. B* **1956**, *69*, 802–807.
18. Kittel, C., *Introduction to Solid State Physics, 7th ed.*; John Wiley and Sons, Inc.: New York, 1996.
19. Zaky, A. A.; Hawley, R., *Dielectric Solids;* Dover Publications Inc.: New York, 1970.
20. Lichtenecker, K. Dielectric Constant of Natural and Synthetic Mixtures. *Phys. Zeit.* **1926**, *27*, 115–158.
21. Aspnes, D. E. Local-Field Effects and Effective-Medium Theory: A Microscopic Perspective. *Am. J. Phys.* **1982**, *50*, 704–709.
22. Li, J. Y.; Zhang, L.; Duchame, S. Electric Energy Density of Dielectric Nanocomposites. *Appl. Phys. Lett.* **2007**, *90*, 132901.
23. Li, J. Y.; Huang, C.; Zhang, Q. Enhanced Electromechanical Properties in All-Polymer Percolative Composites. *Appl. Phys. Lett.* **2004**, *84*, 3124–3126.
24. Paniagua, S. A.; Hotchkiss, P. J.; Jones, S. C.; Marder, S. R.; Mudalige, A.; Marrikar, F. S.; Pemberton, J. E.; Armstrong, N. R. Phosphonic Acid Modification of Indium-Tin Oxide Electrodes: Combined XPS/UPS/Contact Angle Studies. *J. Phys. Chem. C* **2008**, *112*, 7809–7817.
25. Bars, N. L.; Tinet, D.; Faugere, A. M.; Damme, H. V.; Levitz, P. Adsorption Mechanism of Ester Phosphate on Baryum Titanate in Organic Medium. Preliminary Results on the Structure of the Adsorbed Layer. *J. Phys. III* **1991**, *1*, 707–718.
26. Gao, W.; Dickinson, L.; Grozinger, C.; Morin, F. G.; Reven, L. Self-Assembled Monolayers of Alkylphosphonic Acids on Metal Oxides. *Langmuir* **1996**, *12*, 6429–6435.
27. The permittivity for BT was adjusted as a best fit value based on the measured permittivity of P(VDF-HFP) from a set of thin film capacitor devices. Though there are literatures reporting permittivities for sintered BT nanoparticles with grain size of 50 nm, there is a lack of permittivity data for unsintered dispersed BT nanoparticles of this size.
28. He, X.; Yao, K.; Gan, B. K. Phase Transition and Properties of a Ferroelectric Poly(vinylidenefluoride-hexafluoropropylene) Copolymer. *J. Appl. Phys.* **2005**, *97*, 084101.
29. Malyshkina, I. A.; Markin, G. V.; Kochervinskii, V. V. Investigation into the Dielectric Relaxation of Vinylidene Fluoride Copolymers with Hexafluoropropylene. *Phys. Solid State* **2006**, *48*, 1197–1199.
30. Zhao, Z.; Buscaglia, V.; Viviani, M.; Buscaglia, M. T.; Mitoseriu, L.; Testino, A.; Nygren, M.; Johnsson, M.; Nanni, P. Grain-Size Effects on the Ferroelectric Behavior of Dense Nanocrystalline $BaTiO_3$ Ceramics. *Phys. Rev. B* **2004**, *70*, 024107.
31. Petrovsky, V.; Petrovsky, T.; Kamlapurkar, S.; Dogan, F. Dielectric Constant of Barium Titanate Powders Near Curie Temperature. *J. Am. Ceram. Soc.* **2008**, *91*, 3590–3592.
32. Weibull, W. A Statistical Distribution Function of Wide Applicability. *J. Appl. Mech.* **1951**, *18*, 293–297.
33. Tuncer, E.; James, D. R.; Sauers, I.; Ellis, A. R.; Pace, M. O. On Dielectric Breakdown Statistics. *J. Phys. D* **2006**, *39*, 4257–4268.
34. Tuncer, E.; Sauers, I.; James, D. R.; Ellis, A. R.; Paranthaman, M. P.; Aytug, T.; Sathyamurthy, S.; More, K. L.; Li, J.; Goyal, A. Electrical Properties of Epoxy Resin Based Nano-Composites. *Nanotechnology* **2007**, *18*, 025703.
35. Davies, W. E. V. J.; Dutton, J.; Harris, F. M.; Jones, F. L. Electrical Breakdown of Air at High Voltages. *Nature* **1965**, *205*, 1092–1093.
36. Tuncer, E.; Sauers, I.; James, D. R.; Ellis, A. R.; Paranthaman, M. P.; Goyal, A.; More, K. L. Enhancement of Dielectric Strength in Nanocomposites. *Nanotechnology* **2007**, *18*, 325704.
37. O'Dwyer, J. J., *The Theory of Dielectric Breakdown of Solids;* Oxford University Press: London, 1964.
38. Rice, R. W., *Porosity of Ceramics;* Marcel Dekker, Inc.: New York, 1998.